Journal of Statistical Physics, Vol. 28, No. 2, 1982

A Monte Carlo Study of the Classical Two-Dimensional One-Component Plasma

J. M. Caillol,[1] D. Levesque,[1] J. J. Weis,[1] and J. P. Hansen[2]

Received December 2, 1981

We present results from extensive Monte Carlo simulations of the fluid phase of the two-dimensional classical one-component plasma (OCP). The difficulties associated with the infinite range of the logarithmic Coulomb interaction are eliminated by confining the particles to the surface of a sphere. The results are compared to those obtained for a planar system with screened Coulomb interactions and periodic boundary conditions; in this case the infinite tail of the Coulomb interaction is treated as a perturbation. The "exact" simulation results are used to test various approximate theories, including a semiempirical modification of the hypernetted-chain (HNC) integral equation. The OCP freezing transition is located at a coupling $\Gamma = e^2/k_B T \simeq 140$.

KEY WORDS: Two-dimensional classical one-component plasma; freezing transition; Monte Carlo simulation; modified hypernetted-chain integral equation.

1. INTRODUCTION

The one-component plasma (OCP) in d dimensions is a system of identical point particles carrying a charge e and interacting through the d-dimensional Coulomb potential; to ensure charge neutrality the particles are immersed in a uniform background of opposite charge. The Coulomb potential $v(r)$ in d dimensions is the solution of Poisson's equation:

$$\Delta v(r) = -2\pi^{d/2}\left[\Gamma(d/2)\right]^{-1} e^2 \delta(\mathbf{r}) \tag{1.1}$$

where Δ denotes the d-dimensional Laplace operator. The OCP is the

[1] Laboratoire de Physique Théorique et Hautes Energies, Université de Paris-Sud, 91405 Orsay, France; Laboratoire Associé au Centre National de la Recherche Scientifique.

[2] Laboratoire de Physique Théorique des Liquides*, Université Pierre et Marie Curie, 75230 Paris Cedex 05, France; Equipe Associée au Centre National de la Recherche Scientifique.

0022-4715/82/0600-0325$03.00/0

simplest possible model of a continuous Coulomb fluid and is hence of considerable theoretical importance. The static and dynamic properties of the three-dimensional (3d) OCP have been thoroughly investigated in view of its relevance for the description of dense plasmas.[1,2] The two-dimensional (2d) version has recently received much attention, and a number of exact and approximate theoretical results concerning the static structure and the thermodynamics of this model are by now available. In this paper we present extensive Monte Carlo results for these properties in order to provide a reliable test of approximate theoretical calculations and to allow a precise location of the fluid–solid transition for this model.

In order to overcome the usual difficulties linked to the small size of the computer-simulated systems and the infinite range of the Coulomb potential, we have used two very different Monte Carlo schemes which lead to mutually compatible results and give us some confidence that the statistical averages which we quote are close to their thermodynamic limit. The paper is organized as follows. In Section 2 all relevant quantities are defined and the essential results previously known for the 2d OCP are briefly summarized. In Sections 3 and 4 we describe the two Monte Carlo schemes which we have used and compare the data which they yield. Section 5 is devoted to a critical examination of the "best" available theoretical scheme, the hypernetted chain (HNC) equation and its extensions. The fluid–solid transition is discussed in Section 6, while some concluding remarks are contained in Section 7.

2. DEFINITIONS AND GENERAL PROPERTIES

The solution of Eq. (1.1) in two dimensions is

$$v(r) = -e^2 \ln(r/L) \tag{2.1}$$

where L is an arbitrary scaling length. Let $n = N/S$ be the number density, with N the total number of particles and S the area of the system. A convenient unit of length is the "ion-disk" radius:

$$a = (\pi n)^{-1/2} \tag{2.2}$$

and in the following it will be convenient to choose $L = a$, and to use reduced distances $x = r/a$. If the N particles are confined to a disk of radius R uniformly filled by the neutralizing background, the total potential energy in a given configuration is the sum of particle–particle, particle–background and background–background contributions:

$$V_N = -e^2 \sum_{i<j} \ln \frac{r_{ij}}{L} + \frac{Ne^2}{2} \sum_i \left(\frac{r_i}{R} \right)^2 + \frac{1}{2} N^2 e^2 \left[\ln\left(\frac{R}{L} \right) - \frac{3}{4} \right] \tag{2.3}$$

where $\mathbf{r}_i$ is the position vector of particle i, as measured from the center of the disk, $r_i = |\mathbf{r}_i|$ and $r_{ij} = |\mathbf{r}_i - \mathbf{r}_j|$. An equilibrium state of the 2d OCP is entirely characterized by the single dimensionless coupling constant:

$$\Gamma = e^2/k_B T \tag{2.4}$$

which is independent of density.

If $g(r)$ denotes the pair distribution function and $h(r) = g(r) - 1$ the pair correlation function, charge neutrality implies that

$$2\pi n \int_0^\infty h(r) r\, dr = 2 \int_0^\infty h(x) x\, dx = -1 \tag{2.5}$$

The virial equation combined with Eq. (2.5) immediately yields the equation of state:[3]

$$\frac{\beta P}{n} = 1 - \frac{\beta e^2}{4} = 1 - \frac{\Gamma}{4} \tag{2.6}$$

where $\beta = 1/k_B T$. This exact result is a simple consequence of the observation that the density is an irrelevant variable for a system of particles interacting through the logarithmic potential (2.1). The excess internal energy U^{ex}, on the other hand, is a nontrivial quantity which can be calculated from $h(r)$ via the energy equation:

$$\begin{aligned} u(\Gamma) = \frac{U^{\text{ex}}}{Ne^2} &= -\pi n \int_0^\infty h(r) \ln\left(\frac{r}{L}\right) r\, dr \\ &= -\int_0^\infty h(x) \ln(x) x\, dx \end{aligned} \tag{2.7}$$

The excess free energy F^{ex} follows then by thermodynamic integration:

$$\begin{aligned} \frac{F^{\text{ex}}}{Ne^2} &= -\frac{1}{4} \ln(\pi n L^2) + f(\Gamma) \\ f(\Gamma) &= \frac{1}{\Gamma} \left[\Gamma_0 f(\Gamma_0) + \int_{\Gamma_0}^{\Gamma} u(\Gamma')\, d\Gamma' \right] \end{aligned} \tag{2.8}$$

The isothermal compressibility, on the other hand, follows directly from the equation of state (2.6):

$$\chi_T^{-1} = \left(\frac{\partial \beta P}{\partial n} \right)_T = 1 - \frac{\Gamma}{4} \tag{2.9}$$

The static structure factor is defined, as usual, by

$$S(k) = 1 + \hat{h}(k) \tag{2.10}$$

where $\hat{h}(k)$ denotes the dimensionless Fourier transform of the pair correla-

tion function:

$$\hat{h}(k) = n\int h(r)\exp(i\mathbf{k}\cdot\mathbf{r})\,d^2r$$

$$= 2\pi n\int_0^\infty h(r)J_0(kr)r\,dr \tag{2.11}$$

with J_0, the zeroth-order cylindrical Bessel function. Via the Ornstein–Zernike relation we introduce the direct correlation function, in k space,

$$\hat{c}(k) = 1 - \left[S(k)\right]^{-1} \tag{2.12}$$

Since for small k (i.e., large r), $\hat{c}(k)$ is expected to behave asymptotically as

$$\hat{c}(k) \underset{k\to 0}{\simeq} -\beta\hat{v}(k) = -\frac{k_D^2}{k^2} \tag{2.13}$$

with $k_D = 1/\lambda_D = (2\pi\beta ne^2)^{1/2}$ the inverse Debye length, it is convenient to separate $\hat{c}(k)$ into its singular and regular parts:[1]

$$\hat{c}(k) = -\frac{k_D^2}{k^2} + \hat{c}^R(k) \tag{2.14}$$

The compressibility equation, as adapted to the OCP, reads[1]

$$\lim_{k\to 0}\hat{c}^R(k) = 1 - \chi_T^{-1} \tag{2.15}$$

It is easy to check that Eqs. (2.12)–(2.15) imply the following additional moment sum rules for the pair correlation function:

$$2\pi n\int_0^\infty h(r)r^2r\,dr = 2a^2\int_0^\infty h(x)x^3\,dx = -4\lambda_D^2 \tag{2.16}$$

$$2\pi n\int_0^\infty h(r)r^4r\,dr = 2a^4\int_0^\infty h(x)x^5\,dx = -64\lambda_D^4\chi_T^{-1} \tag{2.17}$$

Equation (2.16) is also known as the "perfect screening" condition.

In the weak coupling limit ($\Gamma \ll 1$), the static properties of the OCP reduce to their Debye–Hückel (DH) approximation, which amounts to neglecting the regular part of the direct correlation function in Eq. (2.14). The resulting static structure factor takes then the familiar form

$$S_{\mathrm{DH}}(k) = \frac{k^2}{k^2 + k_D^2} \tag{2.18}$$

while the pair correlation function reads

$$h_{\mathrm{DH}}(r) = -\Gamma K_0(r/\lambda_D) \tag{2.19}$$

where K_0 denotes the zeroth-order modified Bessel function of the second kind. The DH excess internal energy is then readily calculated from Eqs.

(2.7) and (2.19) with the result[4]

$$u_{\mathrm{DH}}(\Gamma) = -\tfrac{1}{4}\left[\ln\left(\tfrac{1}{2}\Gamma\right) + 2\gamma\right] \tag{2.20}$$

where $\gamma = 0.57721\ldots$ is Euler's constant, and we have chosen $L = a$. The corresponding excess free energy follows from Eq. (2.8) (with $\Gamma_0 = 0$):

$$f_{\mathrm{DH}}(\Gamma) = -\tfrac{1}{4}\left[\ln\left(\tfrac{1}{2}\Gamma\right) + 2\gamma - 1\right] \tag{2.21}$$

As Γ is increased towards the intermediate coupling regime ($\Gamma \simeq 1$), the DH approximation becomes rapidly questionable, and a number of theoretical schemes have been tried to predict the static properties of the 2d OCP. The so-called STLS approximation[5] (a generalization of the random phase approximation) can be solved exactly in this case, and leads to the following expressions for the internal and free energies:[6]

$$u_{\mathrm{STLS}}(\Gamma) = -\frac{1}{4}\left[2\gamma + \ln\left(\frac{\Gamma}{\Gamma+2}\right)\right] \tag{2.22}$$

$$f_{\mathrm{STLS}}(\Gamma) = -\frac{1}{4}\left\{2\gamma + \ln\left[\frac{\Gamma}{\Gamma+2}\left(\frac{2}{\Gamma+2}\right)^{2/\Gamma}\right]\right\} \tag{2.23}$$

An improvement over STLS theory, due to Totsuji and Ichimaru (TI),[7] has been investigated numerically by Bakshi *et al.*[8] in the intermediate coupling regime of the 2d OCP, where its results agree reasonably well with the predictions of hypernetted chain (HNC) theory. The HNC calculations have since been extended to strong couplings[9] and will be discussed in Section 5.

The most interesting feature in the intermediate coupling regime is the fact that the partition function, and hence the thermodynamics and the distribution functions can be calculated *exactly* for one special value of the coupling constant, namely, $\Gamma = 2$.[10,11] In particular the pair correlation function reduces to a Gaussian:

$$h_{\Gamma=2}(x) = -\exp(-x^2) \tag{2.24}$$

This important result provides a stringent test for any approximate theory. The results of an expansion of the pair correlation function in powers of $(\Gamma - 2)$[11] make it very plausible that the character of $h(r)$ changes from a monotonous behavior, typical of weak coupling, to an oscillatory behavior, characteristic of short-range order, precisely at $\Gamma = 2$.

In the strong coupling limit ($\Gamma \gg 1$), we expect the OCP thermodynamic functions to approach the predictions of the simple "ion disk" (ID) (or circular Wigner–Seitz) model; in particular

$$u_{\mathrm{ID}}(\Gamma) = f_{\mathrm{ID}}(\Gamma) = -\tfrac{3}{8} \tag{2.25}$$

For sufficiently high values of Γ the 2d OCP is expected to crystallize; this point will be investigated in Section 6.

For any coupling the excess internal energy is bounded below by its Debye–Hückel[12] and ion–disk[13] values:

$$u(\Gamma) \geqslant u_{\mathrm{DH}}(\Gamma) = -\tfrac{1}{4}\left[\ln\left(\tfrac{1}{2}\Gamma\right) + 2\gamma\right] \tag{2.25a}$$

$$u(\Gamma) \geqslant u_{\mathrm{ID}}(\Gamma) = -\tfrac{3}{8} \tag{2.25b}$$

The two lower bounds intersect at $\Gamma \simeq 2.8$, and in this intermediate coupling range neither bound is expected to be useful; in particular at $\Gamma = 2$, $u_{\mathrm{DH}} = -0.2886$, $u_{\mathrm{ID}} = -0.375$, while the exact result[10] is $u = -0.0721$. Totsuji[14] proposed a systematic interpolation scheme which provides improved lower bounds in the intermediate coupling regime; for $\Gamma = 2$ his lower bound is -0.2112. Totsuji's scheme has been further improved by Rosenfeld, but no numerical results are available.[15]

3. MONTE CARLO RESULTS ON A SPHERE

The principal aim of this paper is to provide reliable Monte Carlo data for the 2d OCP over a wide range of couplings ($0.5 < \Gamma < 200$). Since only relatively small systems (with $N \simeq 10^2$ particles) can be simulated, the infinite range of the Coulomb potential poses severe truncation problems which are well known from the 3d case. Navet and Jamin[16] simulated systems with free boundaries (N particles in a disk, with the outer shells kept fixed) and an initial triangular lattice configuration; they observed melting of the Coulomb crystal as Γ was lowered below $\Gamma \simeq 100$, but did not discuss the N dependence of their results, which is expected to be severe with free boundary conditions. The usual way of eliminating most of the N dependence is to use periodic boundary conditions in conjunction with Ewald summations of the interactions over the infinite array of periodic images.[17] This procedure has been extensively used in 3d, but it is very cumbersome and time consuming, and was discarded in the present work. Instead we have used two alternative procedures to eliminate the difficulties associated with the boundaries. In the first scheme we have eliminated the boundaries completely by confining the N particles to the surface of a sphere.[18] The second procedure amounts to simulating a periodic system of particles interacting by a short-range screened Coulomb potential and treating the difference between bare and screened potentials as a perturbation.[19] The results of the first method are presented in this section, while the second procedure is examined in the following section.

The method of confining N particles to the surface of a sphere has been successfully applied in Ref. 18 in a "molecular dynamics" simulation

of the 2d classical electron gas, i.e., a system of particles interacting through the 3d Coulomb potential $\sim 1/r$. The pair distribution functions and velocity autocorrelation functions computed on the sphere are indistinguishable from the data obtained from a more conventional plane periodic system with Ewald summations.[20,21]

The procedure of Ref. 18 must be slightly modified to be applicable to the 2d OCP. Let R be the radius of the sphere centered in 0; the number density is $n = N/4\pi R^2$. The position of each particle on the sphere is determined by two polar angles, or equivalently by a radial unit vector $\mathbf{u}$. The mutual distance between two particles i and j is measured along the geodesic:

$$d_{ij} = R\psi_{ij} \tag{3.1a}$$

with

$$\psi_{ij} = \arccos(\mathbf{u}_i \cdot \mathbf{u}_j) \tag{3.1b}$$

The solution of Poisson's equation on the sphere leads to the Coulomb potential:

$$v(\psi_{ij}) = -e^2 \ln\left[\tan(\psi_{ij}/2)\right] \tag{3.2}$$

This form is useless since it is singular for particles on opposite poles ($\psi_{ij} = \pi$), a situation which corresponds to infinitely distant particles in the planar case. For that reason we replace the interactions along the surface of the sphere by interactions along the chords joining the particles on the sphere, i.e., we choose

$$v(\psi_{ij}) = v(r_{ij}) = -e^2 \ln(r_{ij}/L) \tag{3.3a}$$

where r_{ij} is the length of the chord joining particles i and j:

$$r_{ij} = 2R \sin(\psi_{ij}/2) \tag{3.3b}$$

The total potential energy of the N particles and the neutralizing background reads

$$V_N = -\frac{e^2}{2} \sum_{i<j} \ln\left[\frac{2R^2}{L^2}(1 - \cos\psi_{ij})\right] - \frac{N^2 e^2}{4}\left[1 - \ln\left(\frac{4R^2}{L^2}\right)\right] \tag{3.4}$$

It has been shown[22] that the thermodynamic limit (N, $R \to \infty$, n constant) of this system and of the corresponding planar system coincide for the particular state $\Gamma = 2$, where the partition function can be calculated exactly in both cases. The N dependence of the excess free energy per particle has been shown to be $O(\log N/N)$ for $\Gamma = 2$;[22] in Appendix A we show that the N dependence of the corresponding excess internal energy per particle is $O(1/N)$. It is reasonable to assume that the equivalence of the two thermodynamic limits, as well as the N dependence of the energies,

which has been proved rigorously only for $\Gamma = 2$, will remain true for other couplings as well.

Once the spherical geometry has been adopted, the standard Metropolis Monte Carlo method proceeds as usual.[23] We computed the pair distribution function, the excess internal energy, and the excess specific heat at constant volume for several states in the range $0.5 \leqslant \Gamma \leqslant 200$; the results are summarized in Table I and in Figs. 1 and 2. The charge neutrality condition (2.5) is trivially satisfied in the simulations so that they automatically yield the exact equation of state (2.5). The short Monte Carlo run at $\Gamma = 2$ leads to results in excellent agreement with the exact predictions $u_{\Gamma=2} = -0.0721$ and $g_{\Gamma=2}(x)$ given by Eq. (2.24) (cf. Fig. 1). Because static correlations extend further out with increasing Γ, we have systematically increased the system size from $N = 104$ for $\Gamma \leqslant 40$ to $N = 256$ for $\Gamma \geqslant 160$. At $\Gamma = 160$ we checked the N dependence by running two different sizes ($N = 160$ and $N = 256$); no significant differences were detected.

We have calculated the static structure factor from the pair distribution function by a generalization of the Fourier transform (2.11) appropriate for the spherical geometry:[18]

$$S(k) = 1 + 2\pi nR^2 \int_0^{\pi} [\, g(R\theta) - 1] \sin\theta J_0(kR\theta)\, d\theta \tag{3.5}$$

Examples of calculated structure factors are shown in Figs. 3 and 4.

Table I. Monte Carlo Results for the Two-Dimensional OCP on a Sphere[a]

Γ	N	NC	u	C_v^{MC}	C_v, Eq. (3.7)
0.5	104	5×10^5	+ 0.098		
2.	104	1.25×10^5	− 0.1454	0.28	0.280
5.	104	5×10^5	− 0.2488	0.43	0.437
10.	104	5×10^5	− 0.2976	0.59	0.557
20.	104	5×10^5	− 0.3284	0.70	0.688
40.	104	10^6	− 0.3469	0.94	0.836
80.	160	10^6	− 0.3582	1.3	1.009
100.	160	10^6	− 0.3611	1.6	1.071
120.	160	10^6	− 0.3627	2.75	1.124
140.	160	8×10^5	− 0.3643	2.15	1.171
160.	160	5×10^5	− 0.3653	2.9	1.213
160.	256	10^6	− 0.3653	4.1	1.213
200.	256	10^6	− 0.3667	4.1	1.287

[a] N is the number of particles on the sphere, NC the number of MC configurations generated.

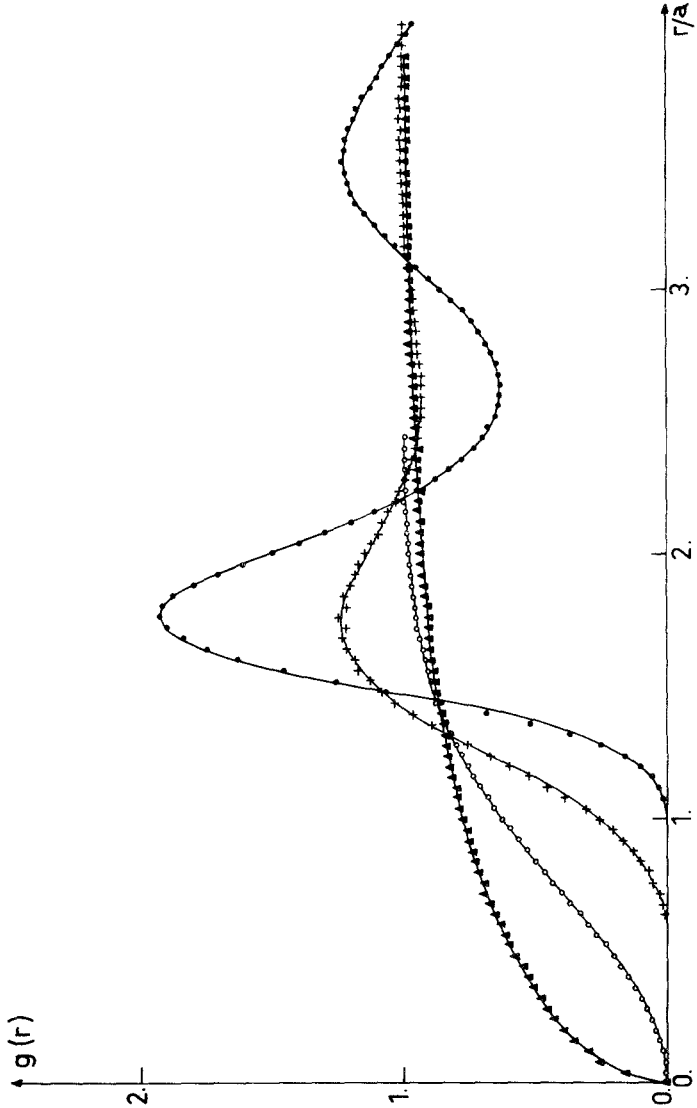

Fig. 1. Pair distribution function $g(r)$ versus $x = r/a$, from the Monte Carlo simulations on a sphere at $\Gamma = 0.5$ (triangles), $\Gamma = 2$ (circles), $\Gamma = 10$ (crosses), and $\Gamma = 40$ (dots).

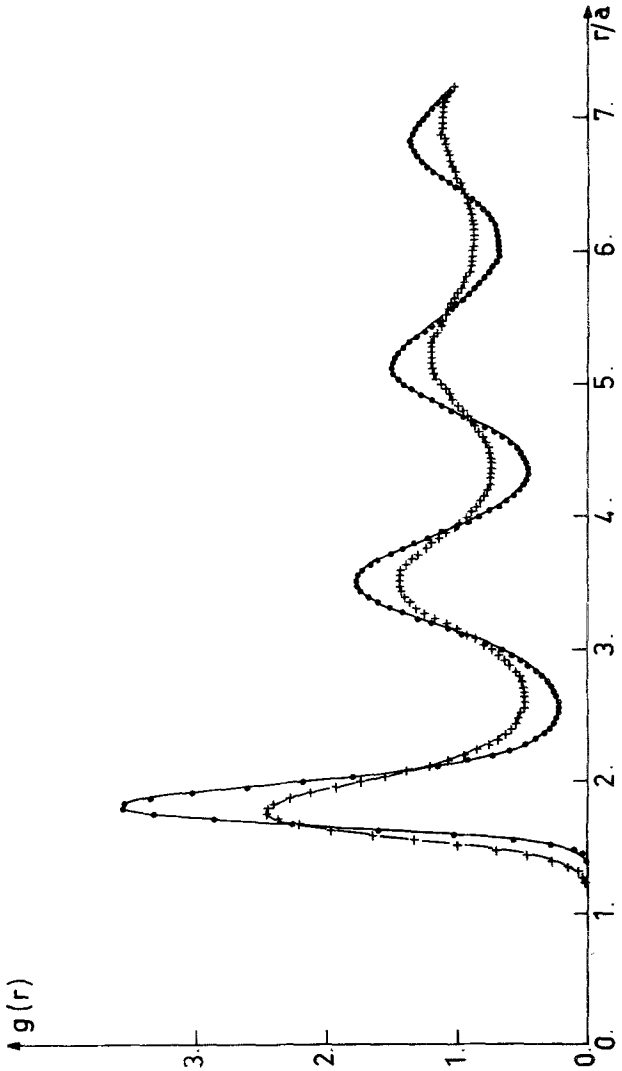

Fig. 2. Same as Fig. 1 for $\Gamma = 80$ (crosses) and $\Gamma = 200$ (dots).

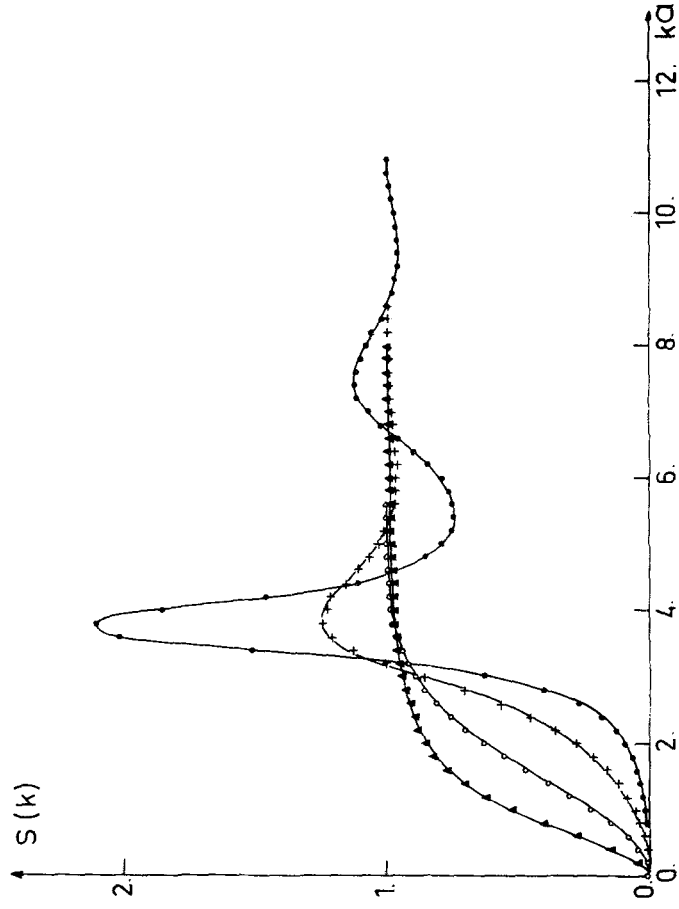

Fig. 3. Static structure factor $S(k)$ versus $q = k \cdot a$; symbols have the same meaning as in Fig. 1.

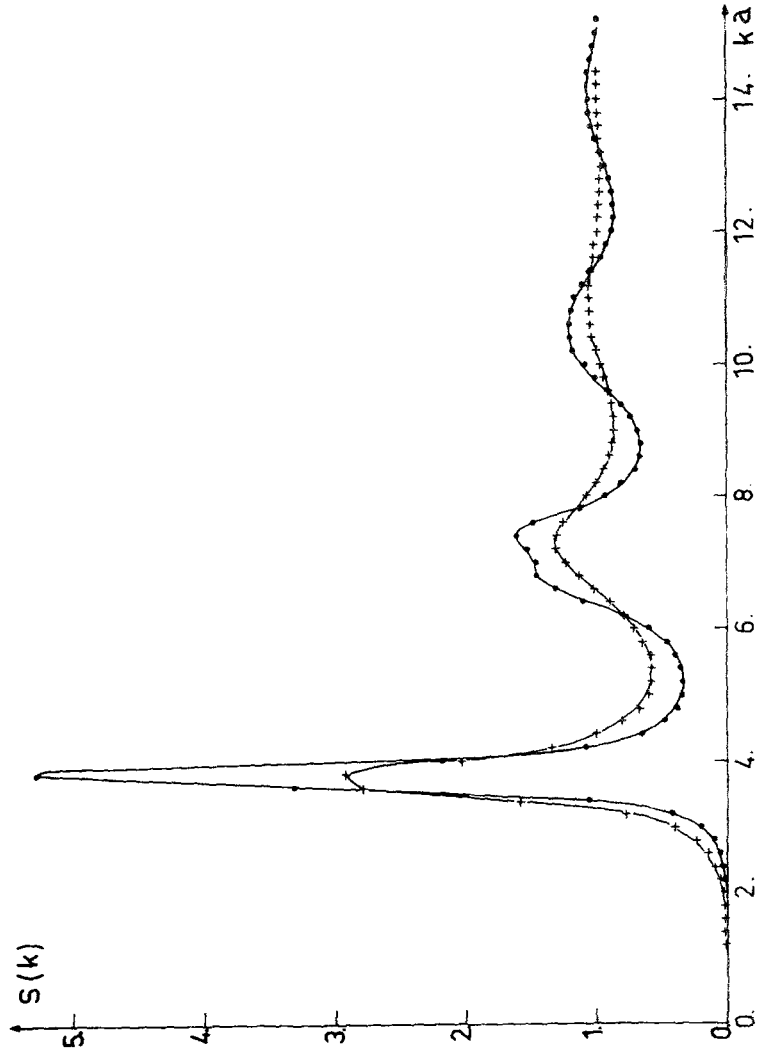

Fig. 4. $S(k)$ versus $q = k \cdot a$; symbols have the same meaning as in Fig. 2.

We have fitted our Monte Carlo energies for $\Gamma \geqslant 2$ by the simple functional form[24]

$$u(\Gamma) = A + \frac{B}{\Gamma^{\alpha}} + \frac{C}{\Gamma^{\gamma}} \tag{3.6}$$

with the following optimal parameters:

$$A = -0.375537, \qquad B = 0.439967, \qquad C = -0.104574$$
$$\alpha = 0.74, \qquad \gamma = 1.7$$

Note that A is very close to its "ion–disk" value -0.375, while the exponent α lies very close to the value -0.75 determined from a similar analysis of the 3d OCP.[24,25] The resulting excess free energy $f(\Gamma)$ follows from Eqs. (3.6) and (2.8) with $\Gamma_0 = 2$ and $f(\Gamma_0) = 0.0455$.[10] The excess specific heat derived from Eq. (3.6) is for $\Gamma \gtrsim 2$

$$C_v(\Gamma) = \frac{C_v}{Nk_B} = -\Gamma^2 \frac{d}{d\Gamma} u(\Gamma)$$
$$= \alpha B \Gamma^{1-\alpha} + \gamma C \Gamma^{1-\gamma} \tag{3.7}$$

The results of Eq. (3.7) are listed in Table I; they differ considerably from the direct Monte Carlo estimates based on the energy fluctuations, at high values of Γ; this discrepancy illustrates the well-known difficulty of obtaining reliable estimates of fluctuations from relatively short Monte Carlo runs. The situation appears to be worse in two than in three dimensions[26] because fluctuations are larger in lower dimensionalities.

4. MONTE CARLO RESULTS IN A PLANE

An alternative scheme, which avoids the cumbersome Ewald summations in planar geometry under periodic boundary conditions, is based on a separation of the Coulomb potential into short-range and long-range parts:[19]

$$v(r) = v_s(r) + v_l(r) \tag{4.1}$$

$v_s(r)$ is chosen such that its magnitude is negligible for separations of the order of $l/2$, where l is the smallest dimension of the basic cell containing the N particles. This means that in a Monte Carlo simulation of a system of particles interacting through the short-range potential only, the simplifying nearest-neighbor convention can be adopted. The long-range part of the potential can be looked upon as a perturbation, the effects of which can be treated by a variety of perturbation schemes; Ceperley and Chester[19] have shown that the reference-hypernetted chain (RHNC) method of Lado[27]

leads to good results for the 3d OCP. Starting from the exact equation[1]

$$g(r) = \exp\left[-\beta v(r) + h(r) - c(r) + B(r)\right] \tag{4.2}$$

where $B(r)$ is the bridge function, the RHNC approximation amounts to replacing $B(r)$ by the corresponding function for the reference system of particles interacting through the potential $v_s(r)$. In other words, given the reference system pair distribution function $g_s(r)$ (obtained from Monte Carlo computations), the coupled equations (2.12) and

$$\frac{g(r)}{g_s(r)} = \exp\left[-\beta v_l(r) + \Delta h(r) - \Delta c(r)\right] \tag{4.3}$$

where $\Delta h = h - h_s$ and $\Delta c = c - c_s$, are solved numerically by iteration. We have adapted Lado's procedure[27,19] to the two-dimensional OCP, choosing for $v_s(r)$ the screened potential:

$$\begin{aligned} v_s(x) &= e^2 K_0(Qx) \\ v_l(x) &= -e^2\left[\ln x + K_0(Qx)\right] \end{aligned} \tag{4.4}$$

$v_s(x)$ reduces to the full Coulomb potential (2.1) at short distances and decreases exponentially at large distances; Q is adjusted such that $v_s \simeq 0$ for $x > l/2a$.

In Fig. 5 we compare the results of this perturbation scheme to the $g(r)$ computed on a sphere at $\Gamma = 120$. The comparison is made for two different cutoffs, $Q = 1.2$ and $Q = 0.8$. In both cases the RHNC approximation is seen to underestimate the correction due to $v_l(r)$, but the results clearly approach the $g(r)$ calculated on the sphere as Q decreases.

5. APPROXIMATE THEORIES

In Section 2 we gave a short list of approximate theories which have been applied to the 2d OCP. Table II compares the excess internal energy $U^{ex}/Ne^2 = u(\Gamma)$ derived from various schemes with our "exact" MC data. The HNC energies[9] are seen to be quite close to the Monte Carlo results over the whole range of Γ values which we have explored. However, HNC theory underestimates the structure of the pair distribution function, as illustrated in Fig. 6 for the case $\Gamma = 40$; this is reminiscent of the situation in 3d.[1] On the other hand, although HNC theory automatically satisfies the moment sum rules (2.5) and (2.16), it predicts compressibilities on the basis of Eq. (2.17) which differ by almost a factor of 2 from the exact result (2.9), underlining the familiar lack of thermodynamic consistency of the theory. Rosenfeld and Ashcroft[28] proposed a semiempirical scheme designed to overcome this inconsistency and improve HNC theory. The latter

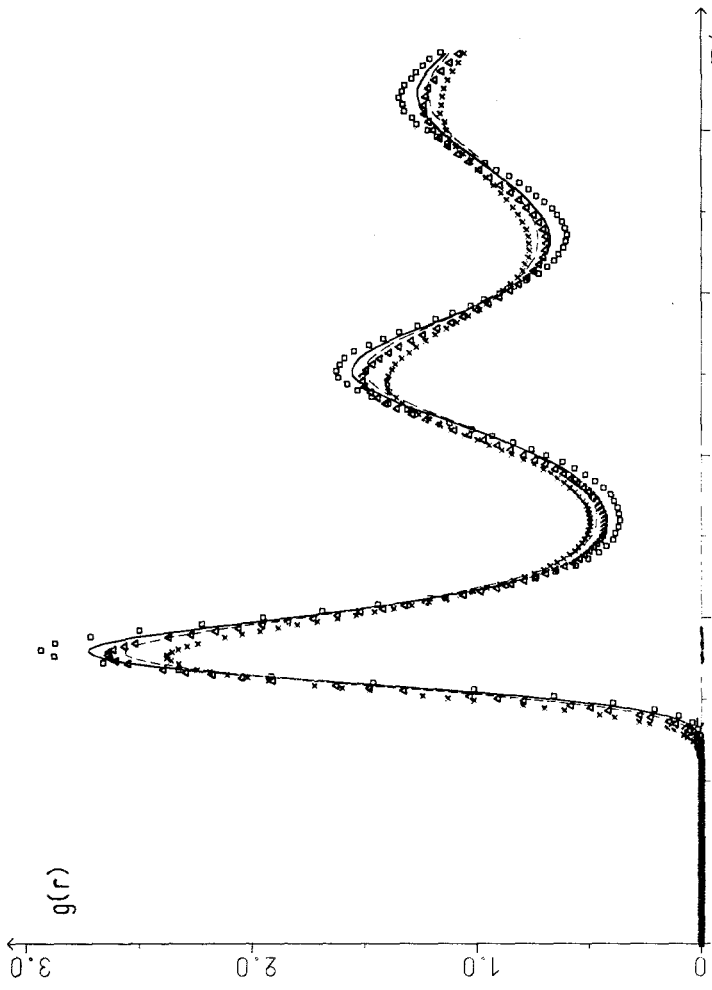

Fig. 5. $g(r)$ at $\Gamma = 120$ versus $x = r/a$. Squares: MC results on a sphere; crosses: MC results in a plane for the screened Coulomb potential (4.4) with $Q = 1.2$; dashed curve: RHNC results for the full Coulomb potential based on the previous MC data; triangles and full curve: same, but with $Q = 0.8$.

Table II. Excess Internal Energy per Particle $u = U^{ex}/Ne^2$ from Our MC Calculations and From Various Theories[a]

Γ	MC	DH	ID	STLS	TI	HNC
0.5	0.098	0.058	−0.375	0.1138	0.1041	0.1036
2.	−0.1454	−0.2886	−0.375	−0.1153	−0.1485	−0.1391
5.	−0.2488	−0.5177	−0.375	−0.2045	−0.2582	−0.2396
10.	−0.2976	−0.6910	−0.375	−0.2430	−0.3093	−0.2879
20.	−0.3284	−0.8643	−0.375	−0.2648	−0.3395	−0.3193
40.	−0.3469	−1.0375	−0.375	−0.2764	−0.3562	−0.3395
80.	−0.3582	−1.2108	−0.375	−0.2824	−0.3649	−0.3523
100.	−0.3611	−1.2666	−0.375	−0.2837	−0.3667	−0.3554
120.	−0.3627	−1.3122	−0.375	−0.2845	−0.3679	−0.3576
140.	−0.3643	−1.3507	−0.375	−0.2851	−0.3688	−0.3592
160.	−0.3653	−1.3841	−0.375	−0.2855	−0.3694	−0.3605
200.	−0.3667	−1.4399	−0.375	−0.2861	−0.3703	−0.3625

[a]HNC results from Ref. 9; STLS results (Ref. 6) from Eq. (2.22); TI results from Ref. 8 (note that the values for $\Gamma \gtrsim 10$ are based on an extrapolation of a fit established for $\Gamma \lesssim 10$); DH: Debye–Hückel lower bound (2.25a); ID: ion–disk lower bound (2.25b).

amounts to setting $B(r) = 0$ in Eq. (4.2) and solving the resulting closed system of Eqs. (4.2) and (2.12) iteratively. In the modified hypernetted chain (MHNC) scheme, $B(r)$ is approximated in Eq. (4.2) by the corresponding function for hard-core particles (hard spheres in 3d, hard disks in 2d). The only free parameter in the problem is the effective packing fraction of the reference hard-core system; this parameter can in principle be adjusted so as to ensure thermodynamic consistency; in practice the effective packing fraction has been adjusted to yield good agreement with Monte Carlo data in an application to the 3d OCP.[28]

While the bridge function $B(r)$ is relatively well known as a function of packing fraction for the hard-sphere fluid, much less information is available for the two-dimensional hard-disk fluid. Consequently we have adapted the MHNC scheme to the present 2d situation, by making use of the exact result at $\Gamma = 2$.[11] From Eq. (2.24) we derive in Appendix B the following form for the direct correlation function $c(x)$ and for the bridge function $B(x)$ at $\Gamma = 2$ ($x = r/a$):

$$c_{\Gamma=2}(x) = -2\gamma - \sum_{j=1}^{\infty} \frac{e^{-x^2/j} - 1}{j} \tag{5.1}$$

$$B_{\Gamma=2}(x) = e^{-x^2} + \ln\left[(1 - e^{-x^2})/x^2\right] + c(x) \tag{5.2}$$

$B(x)$ is very accurately represented by the simple functional form

$$B_{\Gamma=2}(x) = e^{-x^2}\left[B_0 + B_2x^2 + B_4x^4 + B_6x^6\right] \tag{5.3}$$

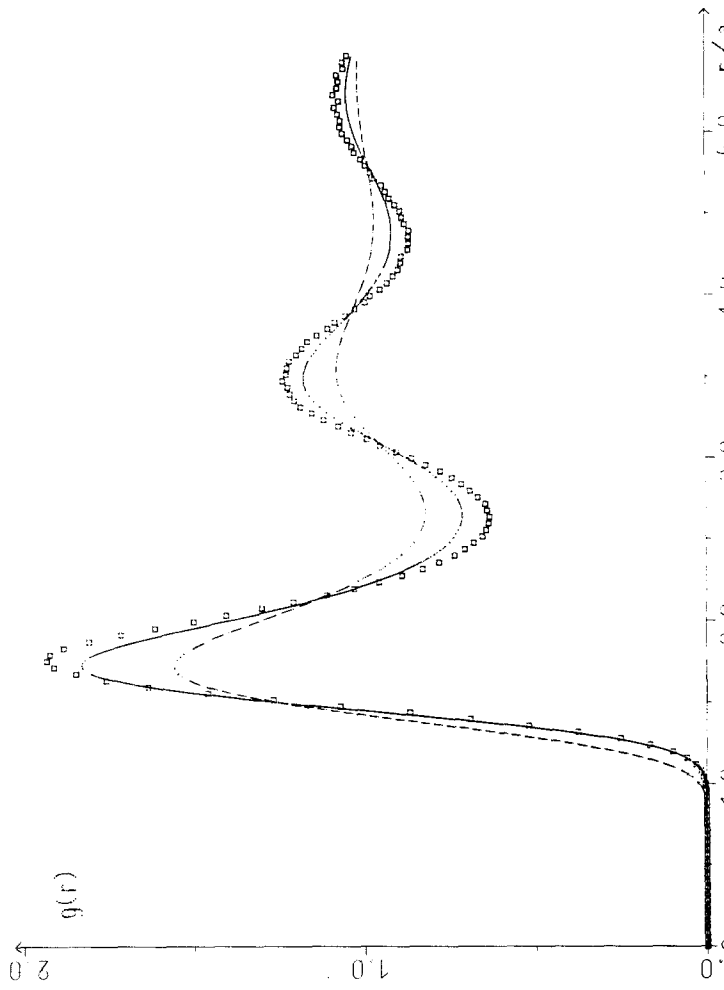

Fig. 6. $g(r)$ versus $x = r/a$ at $\Gamma = 40$; squares: MC result on a sphere; dashed curve: HNC result; full curve: MHNC result.

The coefficients B_{2n} are obtained by identifying the Taylor expansion of Eq. (5.3) with the exact Taylor expansion of $B_{\Gamma=2}(x)$, given in Appendix B:

$$B_0 = b_0 = 1 - 2\gamma = -0.1544313$$

$$B_2 = b_0 + b_2 = -0.00949726$$

$$B_4 = \tfrac{1}{2}b_0 + b_2 + b_4 = 0.00835662$$

$$B_6 = \tfrac{1}{6}b_0 + \tfrac{1}{2}b_2 + b_4 + b_6 = 0.00108723$$

We now make the assumption that the shape of the function $B(x)$ does not change significantly with Γ, but that its amplitude $B(x = 0)$ scales approximately as Γ, a behavior similar to that of $c(x)$.[9] In other words we make the ansatz

$$B_\Gamma(x) = \alpha \tfrac{1}{2}\Gamma B_{\Gamma=2}(x) \tag{5.4}$$

where the coefficient α, which we expect to be of the order of unity, is adjusted to achieve thermodynamic consistency. In practice we have solved the coupled set of MHNC equations (4.2) and (2.12) with $B(x)$ given by Eq. (5.4) for several values of α. The Hankel transform (2.11) was reduced to two successive Fourier transforms by a simple exponential change of variables;[37,38] the Fourier transforms were evaluated numerically by a standard fast Fourier transform routine. The choice $\alpha = 0$ corresponds to the standard HNC equation for which solutions were already available.[9] For a given value of Γ, α was varied until the compressibility calculated from Eq. (2.17) coincided with the exact compressibility (2.9). Results of this procedure are summarized in Table III and in Fig. 6. The improvement over bare HNC theory is impressive, and the thermodynamically consistent MHNC results lie reasonably close to the "exact" Monte Carlo data. The value of α which achieves thermodynamic consistency increases with Γ but has a tendency to saturate for very strong couplings. Although in principle

Table III. Results from MHNC Scheme[a]

Γ	u	χ_T^{exact}	χ_T	α	MC
2	−0.1443	0.50	0.50	1	−0.1454
5	−0.2476	−0.25	−0.25	1.93	−0.2488
10	−0.2964	−1.50	−1.51	2.765	−0.2976
20	−0.3275	−4.00	−4.01	3.70	−0.3284
40	−0.3465	−9.00	−9.01	4.65	−0.3469
60	−0.3539	−14.00	−14.04	5.17	

[a] $u = U^{\text{ex}}/Ne^2$ is the excess internal energy per particle; MC is the "exact" Monte Carlo value of u; α is the value of the parameter in Eq. (5.4) which yields thermodynamic consistency; χ_T is the corresponding inverse isothermal compressibility, which should be compared to its exact value (2.9), χ_T^{exact}.

our procedure could be extended to arbitrarily strong couplings, we have limited ourselves to $\Gamma \leqslant 60$ since we experienced severe convergence problems in the numerical iteration procedure for higher values of Γ.

6. CRYSTALLIZATION

The preliminary Monte Carlo simulations of the 2d OCP with free boundaries, by Navet and Jamin,[16] point towards a stable triangular lattice for $\Gamma \gtrsim 100$, while melting occurs at lower couplings. We have located the fluid–solid phase transition by comparing the free energies of both phases. The free energy of the fluid can be calculated by integrating the internal energy (3.6) according to Eq. (2.8), with $\Gamma_0 = 2$ and $f(\Gamma_0) = 0.0455$.[10] For the excess free energy of the solid we have used the result of a simple harmonic lattice calculation,[10] which yields

$$f(\Gamma) = a + (\ln \Gamma + b)/\Gamma \tag{6.1}$$

where $a = -0.37438$ is the triangular Coulomb lattice sum and $b = -0.262$. Anharmonic contributions are expected to be very small for $\Gamma \gtrsim 100$ as in the 3d OCP,[29] a consequence of the extreme smoothness of the Coulomb potential. When plotted as functions of Γ, the two free-energy curves intersect at $\Gamma = 140$; the fluid phase has the lower free energy and is hence the stable phase, below $\Gamma = 140$, while above that value of the coupling constant the solid is the stable phase. Note that since the coupling is independent of density, the phase transition takes place at constant volume. Although there is no volume change on melting,[30] the phase change at the transition temperature is still first order since there is a nonvanishing latent heat of fusion $l = T\Delta S$. We find $\Delta s = (S_{\text{fluid}} - S_{\text{solid}})/Nk_B = 0.40$, a value close to that found for a 2d system of particles interacting through an inverse twelfth power potential ($\Delta s = 0.34$).[31] Note that a simple comparison of the free energies of the fluid and solid phases does not rule out the possible existence of an intermediate "hexatic" phase, the first-order transition being replaced by a succession of two "continuous" (second-order) transitions.[32]

In Fig. 7 we compare the fluid structure factors of the 2d OCP and of the hard-disk fluid at their respective freezing transitions; the hard-disk fluid is known to coexist with its crystal phase at a packing fraction $\eta = \pi n\sigma^2/4 = 0.69$ (where σ is the disk diameter).[33] Both structure factors are plotted versus the reduced wave number $q = ak$. The main peaks of the two structure factors have a striking resemblance, indicating very similar local structures (or short-range order) near the freezing transition despite the extreme difference between the pair interactions. This "universality" has also been observed in 3d[34] and is the basis of a very simple "freezing criterion,"[35] the two-dimensional version of which can be stated as

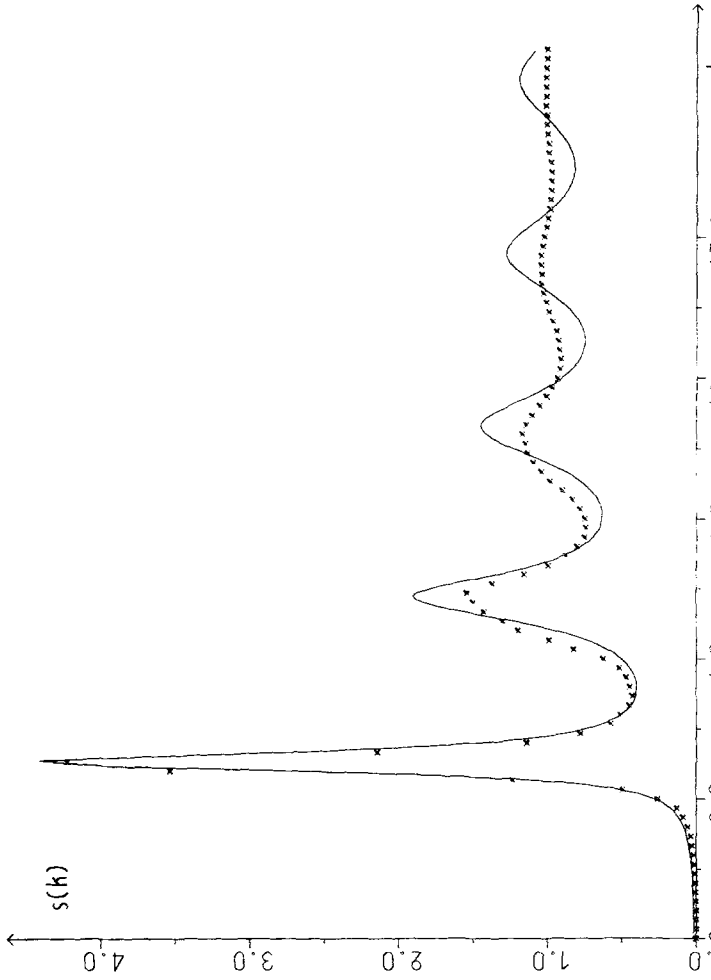

Fig. 7. Static structure factor $S(k)$ versus $q = k \cdot a$ for the hard disk (full curve) and the OCP (crosses) fluids at freezing ($\eta = 0.69$; $\Gamma = 140$).

follows:

> Any classical two-dimensional fluid with central pair interactions freezes whenever the amplitude of the main peak in its static structure factor reaches the corresponding hard-disk value $S(k_0) \simeq 4.4$.

The subsequent oscillations in $S(k)$ are much more damped for the OCP than for the hard-disk fluid, owing to the softness of the Coulomb repulsion compared to the infinite discontinuity of the hard-core repulsion.

Finally it is worth comparing the two- and three-dimensional cases. The 3d OCP crystallizes at $\Gamma = \beta e^2/a$ [with $a = (3/4\pi n)^{1/3}] \simeq 170$,[29,25] a figure close to the value 140 of the 2d coupling constant. As might be expected, the entropy change on melting is larger ($\Delta s \simeq 0.8$) in 3d than in 2d.

7. CONCLUSION

Although it is of limited physical importance, the two-dimensional OCP is an interesting statistical mechanics model because of its great simplicity and because a number of exact results are known for the static properties, which make this model an ideal testing ground for approximate theories. Our Monte Carlo simulations yield a detailed picture of the thermodynamics and of the pair structure of the fluid phase. There are some striking qualitative similarities with the three-dimensional counterpart of the model, a situation which appears to hold for the collective dynamical behavior as well.[36] Knowledge of the exact compressibility for all couplings [Eq. (2.9)] allows a direct implementation of the MHNC scheme which does not rely on a previous knowledge of "exact" simulation data. Although the MHNC results represent a considerable improvement over bare HNC theory, they are not entirely satisfactory, indicating a variation of the *range* and possibly the *shape* of the bridge function with coupling.

Provided the melting transition is always first order in 2d, the physically most interesting result of our work is the indication for the existence of a universal "freezing indicator" based on the amplitude of the main peak in the fluid structure factor. More simulations of various two-dimensional systems near freezing are necessary to confirm the first-order nature of the transition and the validity of the freezing criterion (see, e.g., Ref. 31).

ACKNOWLEDGMENT

The interest and help of Bernard Jancovici throughout this work is gratefully acknowledged. J. P. H. benefited from the hospitality of Philippe Nozières at the Institut Laue Langevin, where part of this work was carried out.

APPENDIX A

The excess internal energy for a system of N particles on a sphere of radius R is, according to Eq. (3.3) and Ref. 22,

$$u_N = \frac{U^{ex}}{Ne^2} = -\pi R^2 n \int_0^\pi [\, g_N(\theta) - 1 \,] \ln\left[\frac{2R}{L} \sin\frac{\theta}{2} \right] \sin\theta \, d\theta \tag{A.1}$$

where $n = N/4\pi R^2$ and $g_N(\theta)$, the pair distribution function for the finite system, has been calculated exactly in Ref. 22 for $\Gamma = 2$:

$$g_N(\theta) - 1 = -\left[\frac{1 + \cos\theta}{2} \right]^{N-1} \tag{A.2}$$

Equation (A.1) can be rewritten as

$$u_N = u_N^{(1)} + u_N^{(2)}$$

with

$$\begin{aligned} u_N^{(1)} &= \frac{N}{4} \int_0^\pi \left[\frac{1 + \cos\theta}{2} \right]^{N-1} \ln\left(\frac{2R}{L} \right) \sin\theta \, d\theta \\ &= \frac{N}{4} \ln\left(\frac{2R}{L} \right) \int_{-1}^{+1} \left(\frac{1 + x}{2} \right)^{N-1} dx \\ &= \frac{1}{4} \ln\left[\frac{N}{\pi n L^2} \right] \end{aligned} \tag{A.3}$$

To calculate $u^{(2)}$, we make the change of variable $y = (1 + \cos\theta)/2$:

$$\begin{aligned} u_N^{(2)} &= \frac{N}{8} \int_0^\pi \left(\frac{1 + \cos\theta}{2} \right)^{N-1} \ln\left(\frac{1 - \cos\theta}{2} \right) \sin\theta \, d\theta \\ &= \frac{N}{4} \int_0^1 y^{N-1} \ln(1 - y) \, dy \end{aligned} \tag{A.4}$$

The integral is readily evaluated by expanding the logarithm

$$\begin{aligned} u_N^{(2)} &= -\frac{N}{4} \sum_{l=1}^{\infty} \frac{1}{l(N + l)} \\ &= -\frac{1}{4} \sum_{l=1}^{\infty} \left(\frac{1}{l} - \frac{1}{N + l} \right) \\ &= -\frac{1}{4} \sum_{l=1}^{N} \frac{1}{l} \end{aligned} \tag{A.5}$$

gathering results

$$u_N = -\frac{1}{4} \left[\ln(\pi n L^2) + \sum_{l=1}^{N} \frac{1}{l} - \ln N \right] \tag{A.6}$$

For large N

$$\sum_{l=1}^{N} \frac{1}{l} - \ln N = \gamma + \frac{1}{2N} + O\left(\frac{1}{N^2}\right) \tag{A.7}$$

In the thermodynamic limit we recover the exact result of Ref. 11:

$$u_\infty = -\tfrac{1}{4}\ln\left[\pi n L^2\right] - \tfrac{1}{4}\gamma \tag{A.8}$$

From Eqs. (A.6)–(A.8) we conclude that

$$u_N = u_\infty + O(1/N)$$

whereas the N dependence of the excess free energy is[22]

$$f_N = f_\infty + O\left(\frac{\ln N}{N}\right) \tag{A.9}$$

APPENDIX B

Using reduced wave numbers $q = ak$ and distances $x = r/a$, the dimensionless Fourier (2.11) transform (FT) of the pair correlation function (2.24) at $\Gamma = 2$ can be cast in the form

$$\hat{h}(q) = e^{-q^2/4} \tag{B.1}$$

and the corresponding FT of the direct correlation function results from Eq. (2.12):

$$\hat{c}(q) = \frac{e^{-q^2/4}}{1 - e^{-q^2/4}} \tag{B.2}$$

The $q \to 0$ singularity of $\hat{c}(q)$ is eliminated by considering the regular part:

$$\hat{c}^R(q) = 4/q^2 - \hat{c}(q) \tag{B.3}$$

In order to evaluate the FT of $\hat{c}^R(q)$ we replace q^2 by $q^2 + \epsilon^2$ in (B.2)–(B.3); the limit $\epsilon \to 0$ will be taken at the end of the calculation:

$$\hat{c}^R(q) = \lim_{\epsilon \to 0}\left[\frac{4}{q^2 + \epsilon^2} - \sum_{j=1}^{\infty} \exp\left(-j\frac{q^2 + \epsilon^2}{4}\right)\right] \tag{B.4}$$

We now take the FT of Eq. (B.4) term by term:

$$c^R(x) = \lim_{\epsilon \to 0}\left[2K_0(\epsilon x) + \sum_{j=1}^{\infty} \frac{1}{j} \exp\left(-j\frac{\epsilon^2}{4} - \frac{x^2}{j}\right)\right] \tag{B.5}$$

and

$$c(x) = c^R(x) + 2\ln x \tag{B.6}$$

Using the limiting behavior of the Bessel function

$$\lim_{x\to 0}\left[K_0(\epsilon x)+\ln x\right]=-\gamma-\ln(\epsilon/2) \tag{B.7}$$

the value of $c(x)$ at the origin is easily calculated as

$$\begin{aligned} c(0) &= \lim_{\epsilon\to 0}\left[-2\gamma-2\ln\frac{\epsilon}{2}-\sum_{j=1}^{\infty}\frac{1}{j}\exp\left(-j\frac{\epsilon^2}{4}\right)\right] \\ &= \lim_{\epsilon\to 0}\left\{-2\gamma-2\ln\frac{\epsilon}{2}+\ln\left[1-e^{-\epsilon^2/4}\right]\right\} \\ &= -2\gamma \end{aligned} \tag{B.8}$$

where γ is Euler's constant. Similarily we derive from Eqs. (B.5)–(B.6):

$$c(x)=-2\gamma-\sum_{j=1}^{\infty}\frac{1}{j}\left(e^{-x^2/j}-1\right) \tag{B.9}$$

Equation (B.9) can be Taylor-expanded in even powers of x as

$$c(x)=-2\gamma-\sum_{n=1}^{\infty}\frac{(-1)^n}{n!}\zeta(n+1)x^{2n} \tag{B.10}$$

where $\zeta(m)$ denotes Riemann's function.

The bridge function at $\Gamma = 2$ follows from Eqs. (4.2), (2.24), and (B.9):

$$B(x)=e^{-x^2}+\ln\left(\frac{1-e^{-x^2}}{x^2}\right)+c(x) \tag{B.11}$$

which can be Taylor-expanded in even powers of x:

$$B(x)=\sum_{n=0}^{\infty}b_{2n}x^{2n} \tag{B.12}$$

The coefficients b_{2n} follow immediately from the corresponding coefficients in Eq. (B.10). In particular

$$b_0=1-2\gamma, \qquad b_2=-\tfrac{3}{2}+\zeta(2)=-\tfrac{3}{2}+\tfrac{1}{6}\pi^2, \qquad \text{etc.}\ldots$$

The bridge function (B.11) is reasonably well approximated by

$$B(x)=b_0e^{-x^2} \tag{B.13}$$

A much more accurate representation is given by Eq. (5.3).

NOTE ADDED IN PROOF

Since this work has been submitted for publication we received notice of a similar study by de Leeuw and Perram based on molecular dynamics simulations with periodic boundary conditions. The results of both calcula-

tions are in excellent agreement. Detailed comparison can be found in the work of de Leeuw and Perram (to appear in *Physica A*).

REFERENCES

1. M. Baus and J. P. Hansen, *Phys. Rep.* **59**:1 (1980).
2. C. Deutsch, Y. Furutani, and M. M. Gombert, *Phys. Rep.* **69**:85 (1981).
3. E. H. Hauge and P. C. Hemmer, *Phys. Norv.* **5**:209 (1971).
4. C. Deutsch, H. E. DeWitt, and Y. Furutani, *Phys. Rev. A* **20**:2631 (1979).
5. K. S. Singwi, M. P. Tosi, R. H. Land, and A. Sjolander, *Phys. Rev.* **176**:589 (1968).
6. R. Calinon, K. I. Golden, G. Kalman, and D. Merlini, *Phys. Rev. A* **20**:329 (1979).
7. H. Totsuji and S. Ichimaru, *Progr. Theor. Phys.* **50**:753 (1973); **52**:42 (1974).
8. P. Bakshi, R. Calinon, K. I. Golden, G. Kalman, and D. Merlini, *Phys. Rev. A* **23**:1915 (1981).
9. J. P. Hansen and D. Levesque, *J. Phys. C* **14**:L603 (1981).
10. A. Alastuey and B. Jancovici, *J. Phys.* **42**:1 (1981).
11. B. Jancovici, *Phys. Rev. Lett.* **46**:386 (1981).
12. N. D. Mermin, *Phys. Rev.* **171**:272 (1968).
13. R. R. Sari and D. Merlini, *J. Stat. Phys.* **14**:91 (1976).
14. H. Totsuji, *Phys. Rev. A* **19**:2433 (1979).
15. Y. Rosenfeld, to be published.
16. M. Navet and E. Jamin, unpublished results.
17. S. G. Brush, H. L. Sahlin, and E. Teller, *J. Chem. Phys.* **45**:2102 (1966).
18. J. P. Hansen, D. Levesque, and J. J. Weis, *Phys. Rev. Lett.* **43**:979 (1979).
19. D. M. Ceperley and G. V. Chester, *Phys. Rev. A* **15**:755 (1977).
20. H. Totsuji, *Phys. Rev. A* **17**:399 (1978); R. C. Gann, S. Chakravarty, and G. V. Chester, *Phys. Rev. B* **20**:326 (1979).
21. R. K. Kalia, P. Vashishta, S. W. de Leeuw, and A. Rahman, *J. Phys. C* **14**:L991 (1981).
22. J. M. Caillol, *J. Phys. Lett. (Paris)* **42**:L245 (1981).
23. N. A. Metropolis, A. W. Rosenbluth, M. N. Rosenbluth, A. M. Teller, and E. Teller, *J. Chem. Phys.* **21**:1087 (1953).
24. H. E. DeWitt, *Phys. Rev. A* **14**:1290 (1976).
25. W. L. Slattery, G. D. Doolen, and H. E. DeWitt, *Phys. Rev. A* **21**:2087 (1980).
26. J. P. Hansen, *Phys. Rev. A* **8**:3096 (1973).
27. F. Lado, *Phys. Rev.* **135**:A1013 (1964).
28. Y. Rosenfeld and N. W. Ashcroft, *Phys. Rev. A* **20**:1208 (1979).
29. E. L. Pollock and J. P. Hansen, *Phys. Rev. A* **8**:3110 (1973).
30. J. D. Weeks, *Phys. Rev. B* **24**:1530 (1981).
31. J. Q. Broughton, G. H. Gilmer, and J. D. Weeks, to be published.
32. D. R. Nelson and B. I. Halperin, *Phys. Rev. B* **19**:2457 (1979).
33. B. J. Alder and T. Wainwright, *Phys. Rev.* **127**:359 (1962).
34. J. P. Hansen and D. Schiff, *Mol. Phys.* **25**:1281 (1973).
35. J. P. Hansen and L. Verlet, *Phys. Rev.* **184**:151 (1969).
36. J. P. Hansen, *J. Phys. Lett. (Paris)* **42**:L397 (1981).
37. J. D. Talman, *J. Comp. Phys.* **29**:35 (1978).
38. J. M. Caillol, D. Levesque, and J. J. Weis, *Mol. Phys.* **44**:733 (1981).